Lab on a Chip

PAPER

View Article Online
View Journal | View Issue

Cite this: *Lab Chip*, 2022, **22**, 2041

Real-time monitoring of epithelial barrier function by impedance spectroscopy in a microfluidic platform†

João Fernandes, [a] Nikita Karra, [a] Joel Bowring, [a] Riccardo Reale, [a] Jonathan James, [b] Cornelia Blume, [bcd] Theresa J. Pell, [e] Wendy C. Rowan, [e] Donna E. Davies, [bcd] Emily J. Swindle [bcd] and Hywel Morgan *[ac]

A multichannel microfluidic platform for real-time monitoring of epithelial barrier integrity by electrical impedance has been developed. Growth and polarization of human epithelial cells from the airway or gastrointestinal tract was continuously monitored over 5 days in 8 parallel, individually perfused microfluidic chips. Electrical impedance data were continuously recorded to monitor cell barrier formation using a low-cost bespoke impedance analyser. Data was analysed using an electric circuit model to extract the equivalent transepithelial electrical resistance and epithelial cell layer capacitance. The cell barrier integrity steadily increased overtime, achieving an average resistance of 418 ± 121 Ω cm^2 (airway cells) or 207 ± 59 Ω cm^2 (gastrointestinal cells) by day 5. The utility of the polarized airway epithelial barrier was demonstrated using a 24 hour challenge with double stranded RNA to mimic viral infection. This caused a rapid decrease in barrier integrity in association with disruption of tight junctions, whereas simultaneous treatment with a corticosteroid reduced this effect. The platform is able to measure barrier integrity in real-time and is scalable, thus has the potential to be used for drug development and testing.

Received 18th November 2021,
Accepted 7th April 2022

DOI: 10.1039/d1lc01046h

rsc.li/loc

1 Introduction

In multicellular organisms, physical barriers comprised of epithelial or endothelial cells are essential for tissue compartmentalization and performance of specialised functions.[1] Epithelial barriers (*e.g.*, the skin, airway and gut) protect tissues from the external environment whereas endothelial barriers separate the blood and tissue compartments. Both barrier cell types elaborate a range of cell–cell adhesion complexes that link with the cytoskeleton to form a robust sheet-like structure that functions as a selective permeability barrier. Key to this function are tight junctions that form between adjacent cells by intercellular transmembrane proteins and intracellular proteins that link to the actin cytoskeleton.[2] These junctions form around the entire perimeter of each cell, forming a continuous belt-like structure to control its barrier (or "gate") properties, thereby regulating paracellular passage of ions, water, and various macromolecules across the epithelial layer. In epithelial cells, tight junctions are concentrated near the apical surface above the adherens junctions (zonula adherens) where they also prevent lateral diffusion and intermixing of molecules in the apical membrane with those in the lateral membrane. This "fence" function maintains cell polarity, another key property for normal epithelial barrier function.

Tight junctions are multimolecular structures which all utilise three types of adhesive transmembrane proteins. These are the MARVEL domain proteins, occludin and tricellulin, the junctional adhesion molecules (JAMs) and the claudins. Claudin domain proteins regulate the permeability selectivity of specific tissue barriers *via* pattern of expression interactions with other claudin family members;[3] this provides the potential to customise their interactions and give rise to the wide range of permselective barriers found in the human micro-environment.[4] The transmembrane proteins of the tight junction link to underlying plaque proteins, such as zona occludin-1 (ZO-1), that in turn associate with the cytoskeleton. These tight junction complexes regulate not only paracellular solute and water flux but also control diverse processes including gene transcription, tumour suppression, cell proliferation, and cell

[a] *Electronics and Computer Science, Faculty of Physical Sciences and Engineering, University of Southampton, UK. E-mail: hm@ecs.soton.ac.uk*
[b] *Clinical and Experimental Sciences, Faculty of Medicine, University of Southampton, UK*
[c] *Institute for Life Sciences, University of Southampton, UK*
[d] *NIHR Southampton Biomedical Research Centre, University Hospital Southampton, UK*
[e] *Novel Human Genetics Research Unit, GlaxoSmithKline R&D, Stevenage, Hertfordshire, UK*

† Electronic supplementary information (ESI) available. See DOI: https://doi.org/10.1039/d1lc01046h

polarity.[5] Given their multifunctional roles, it is perhaps not surprising that epithelial barrier function is dysregulated in a range of diseases including asthma, COPD,[6–10] inflammatory bowel disease and skin diseases such as psoriasis and eczema.[11] Consequently, therapeutic approaches that restore normal barrier function are being actively researched.[12]

Investigations of epithelial barrier integrity typically use *in vitro* models in which cells are grown in standard well plates or on suspended nanoporous supports (Transwell® inserts) where the development and integrity of the epithelial barrier is monitored using transepithelial electrical resistance (TER); the resistance correlates to the number and function of the tight junctions.[13,14] Although TER measurements are easy to perform in Transwell® inserts using Ag/AgCl "chopstick" electrodes, damage to the epithelial layer caused by handling and fluctuations in temperature (removing cells from the incubator) need to be avoided, as these can affect the measurements.[10] Unfortunately, this method does not allow continuous analysis of the cells during formation of the epithelial barrier or modulation following stimulation. Furthermore, the lack of interstitial flow in static Transwell® models does not recapitulate the *in vivo* condition.[15]

Over recent years, organ-on-chip (OoC) models have been developed to address the need for more representative *in vitro* models. These are biomimetic devices that aim to recreate complex organ-level physiological functions, clinically relevant disease phenotypes and pharmacological responses that arise from the structural and functional integration of multiple tissues or interfaces.[15] Several devices have been fabricated to recapitulate epithelial cell barriers *in vitro* models such as skin,[16–18] gut[19] and lungs.[15,20–25] These *in vitro* models are capable of recreating key *in vivo* conditions such as interstitial flow, which supplies metabolites to cells and clears metabolic waste in addition to inducing shear stress on cell cultures (due to liquid flow and pressure differentials), and mechanical stimulation, to mimic breathing motions within alveolus on chip models.[26]

Electrical impedance spectroscopy (EIS) has been used in OoC devices to analyse barrier integrity.[27–30] EIS provides information not only about the epithelial barrier resistance but also epithelial barrier capacitance which correlates with the cell membrane surface area, offering information about cell stacking or development of complex membrane folds such as microvilli.[27] While EIS allows continuous data collection of cell barrier parameters,[27,28,31–34] typically these systems require electrodes on both sides of the barrier (*i.e.*, a *trans* configuration), necessitating the use of submerged conditions to ensure electrical connection to the electrodes. For example, Alexander *et al.*,[35] cultured fibroblasts and EpiDermTM reconstructed human epidermis in an OoC device at an air–liquid interface (ALI), for each TER measurement, the apical layer was temporarily submerged in PBS using an automated pumping system. To solve these issues, we have previously presented a device with the measuring electrodes placed beneath the cell layer (*cis* configuration), allowing continuous monitoring of barrier function at baseline and in response to challenge (Sun *et al.*,[36]). This method was utilised in a lung-on-chip device presented by Mermoud *et al.*,[37] incorporating mechanical stretch and demonstrated frequency-dependent changes in impedance resulting from the detergent permeabilization of the epithelial monolayers.

In this paper we present a barrier on a chip model composed of an 8-channel microfluidic system capable of culturing different types of epithelial cells with integrated real-time impedance capability. Electrical impedance measurements were made using integrated micro-electrodes placed within the basolateral compartment of each chip (directly beneath the cell layer), providing real-time electrical data without perturbation of the cells. Impedance data were fitted to an equivalent circuit model to obtain the TER and epithelial cell layer capacitance. We have demonstrated the establishment of an electrically tight epithelial barrier, in addition to changes in barrier function using a viral mimetic (double stranded RNA (dsRNA)) and reversal of this effect using a corticosteroid, providing proof-of-concept for the system as a drug discovery platform.

1.1 System design

A diagram of the barrier-on-chip system is shown in Fig. 1. A disposable microfluidic chip serves as a simple interchangeable consumable item that interfaces with a microfluidic manifold in a 'plug and play' format (Fig. 1A). The microfluidic chip is secured with magnets, providing an easy, rapid assembly suitable for a non-specialist user. Medium is pumped through individual chips using a syringe pump and a bubble trap, with waste/cellular secretions collected in a tube at the outlet (Fig. 1B). The compact platform accommodates 8 microfluidic chips in parallel, with two systems capable of fitting onto a standard incubator shelf. Syringe pumps used for perfusion of cell culture media are kept outside the incubator (and refrigerated, if required), with the connecting tubing introduced through the door of the incubator.

Details of the microfluidic chip are shown in Fig. 2. It is fabricated from glass and PMMA and is similar in size to a conventional Transwell® and has a cell culture surface area of 0.2 cm^2. The upper (apical) chamber is separated from the lower (basolateral) chamber by a semi-permeable membrane, with a pore diameter of 0.4 μm and pore density of 10^8 pores per cm^2, onto which epithelial cells are grown (Fig. 2B). The base of the chip contains inlet and outlet holes which mate with a microfluidic manifold (Fig. 1B). The support membrane is bonded to a spacer piece approximately 275 μm thick made from self-adhesive tape and PMMA, creating a microfluidic channel through which media flows at a rate of 30 μL h^{-1}. The shape of the microfluidic channel ensures equal flow velocity across the entire cell barrier.[15]

The cells are grown on the apical side of the membrane (Fig. 2A) in a submerged environment (100 μL volume). The chamber is sealed with a thin gas permeable membrane

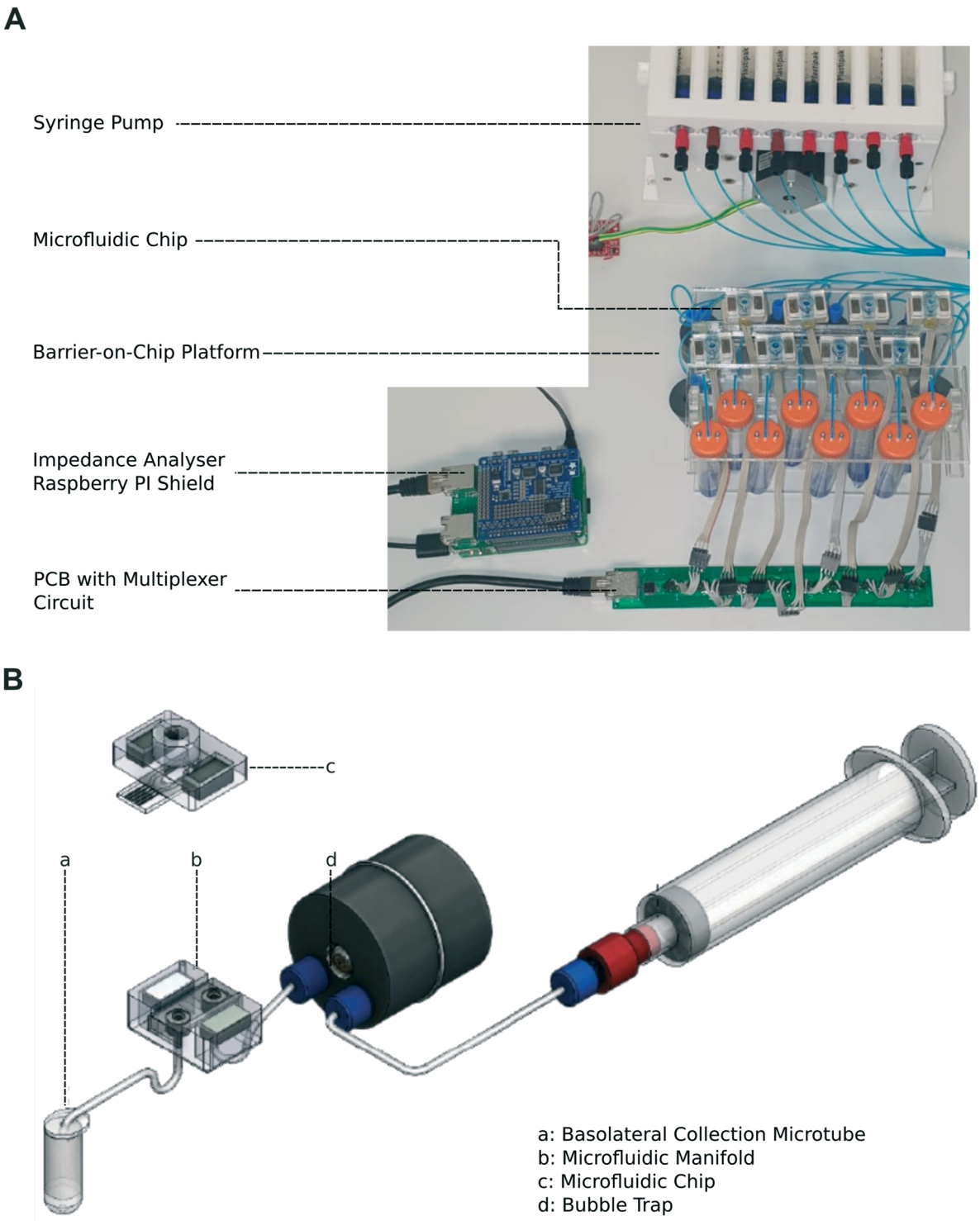

Fig. 1 (A) Photograph of the barrier-on-chip platform with syringe pump and impedance analyser. The eight separate chips are individually connected to a header board. (B) Schematic diagram of one channel. Liquid is pumped from a syringe through a bubble trap and into a manifold that mates with a disposable microfluidic chip clamped to a manifold with magnets.

(PDMS), creating a sterile environment for cell culture and is easily accessible to introduce compounds onto the apical side of the cell culture when required (*via* puncturing). The chip interfaces fluidically with the manifold *via* O-rings and snaps into place using location features and two pairs of magnets.

Each chip has two pairs of electrodes (Fig. 2B) that are used to perform periodical EIS measurements. One pair of electrodes, denominated 'media electrodes' (Fig. 2B), is upstream of the cell electrodes; these measure the electrical properties of the medium, and monitor the system

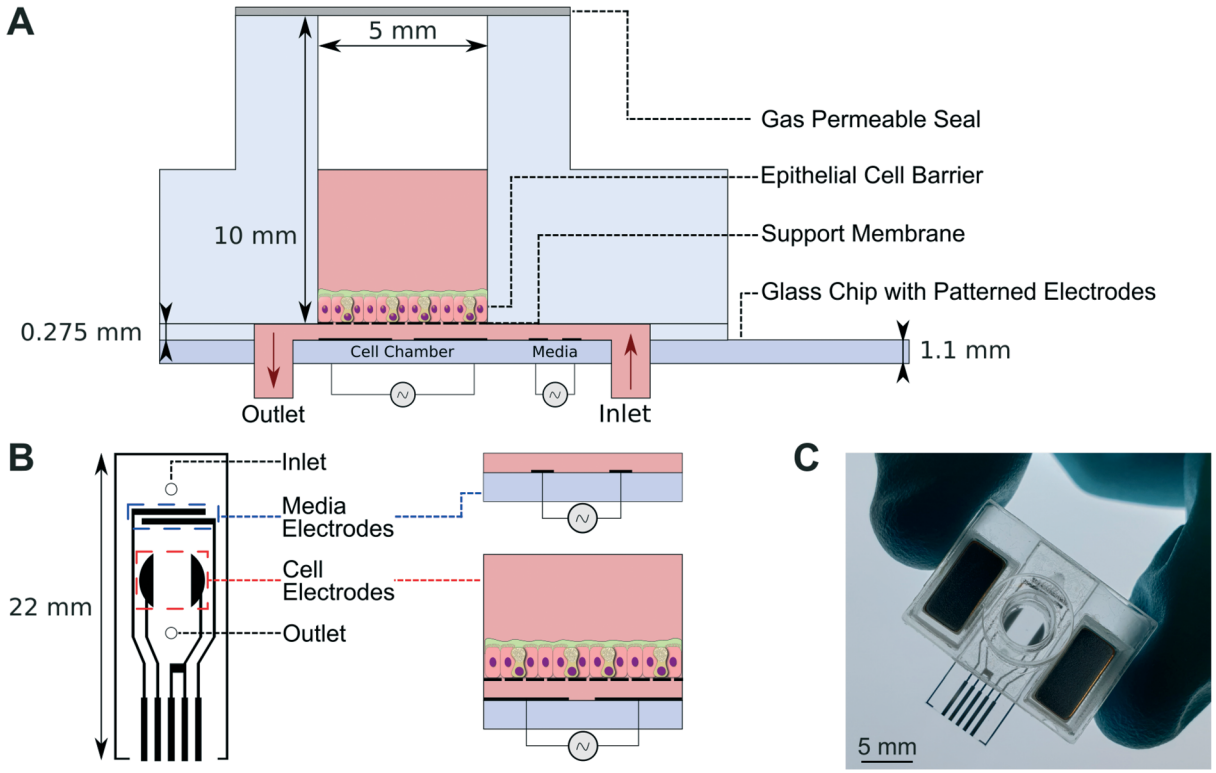

Fig. 2 (A) Cross-section of the microfluidic chip, showing the cell and media electrodes. (B) the arrangement of the two sets of electrodes, together with the position of the fluid inlet and outlet holes. (C) Photograph of a microfluidic chip – the magnets can be seen on either side.

(consistent fluid flow, stability and bubble formation). The electrical parameters of the media measured with these electrodes are used in the circuit model. The second pair of electrodes located beneath the cells ('cell electrodes') measures the electrical properties of the epithelial barrier. The electrical current path between these electrodes is dominated by the basolateral medium, but current also flows through the cell layer. The magnitude of this current depends on the integrity of the cell barrier. This arrangement also allows the 'TER' to be measured at the air–liquid interface as well as the liquid–liquid interface.

In the case of ALI cultures, the presence of air rather than medium on the apical side leads to a high value of apical resistance that could potentially mask the epithelial barrier resistance and capacitance. In practice there is always a layer of fluid or mucus (typically 10 μL) above the cells when grown at ALI.[38] Previous studies by Reale *et al.*,[39] demonstrated the reduction in sensitivity at ALI. Polarized 16HBE14o- cells were grown in Transwell® supports and the volume of apical media reduced to 10 μL before EIS measurement using coplanar electrodes beneath the cell culture. The data is summarized in ESI† Fig. S1 and demonstrates changes in cell barrier can be followed, albeit with reduced sensitivity.

The electrodes in each microfluidic chip are connected to a PCB header board (Fig. 1A) through wires. The PCB routes signals to and from the chips to a custom-made impedance spectrometer based on the AD5933 network analyser IC (Analog devices) controlled with a Raspberry PI expansion board. A custom script written in Python controls the analyser, which can measure the impedance of up to 32 chips in parallel (4 systems). A graphical user interface enables the system to be controlled remotely *via* WiFi, and a screenshot of this display is shown in ESI† Fig. S2. Impedance is measured at 100 mV_{p-p}, between 1 kHz to 100 kHz. This frequency window is sufficient for circuit analysis and characterization of cell barrier resistance and capacitance. In a typical experiment impedance frequency sweeps were recorded automatically at intervals of 17 minutes. Liquid was perfused under the cell layer continuously at a rate of 30 μL per hour.

To minimise toxicity to the cells metal oxide electrodes were used (rather than Ag/AgCl). Specifically, ruthenium oxide which is biocompatible and provides a large effective surface area, similar to platinum black but much more stable minimising electrode polarisation issues.[40]

1.1.1 Electrode design and simulation. In order to extract equivalent TER and cell capacitance from the impedance data, an analytical equivalent circuit model based on Sun *et al.*,[36] was used (Fig. 3). This circuit model comprised elements describing the basolateral medium, the apical medium, the medium inside the nanopores of the Transwell® support membrane and the impedance of the cell barrier. We have improved this method by incorporating an additional pair of electrodes to measure the electrical properties of the cell culture media up-stream of the cell layer. These electrodes

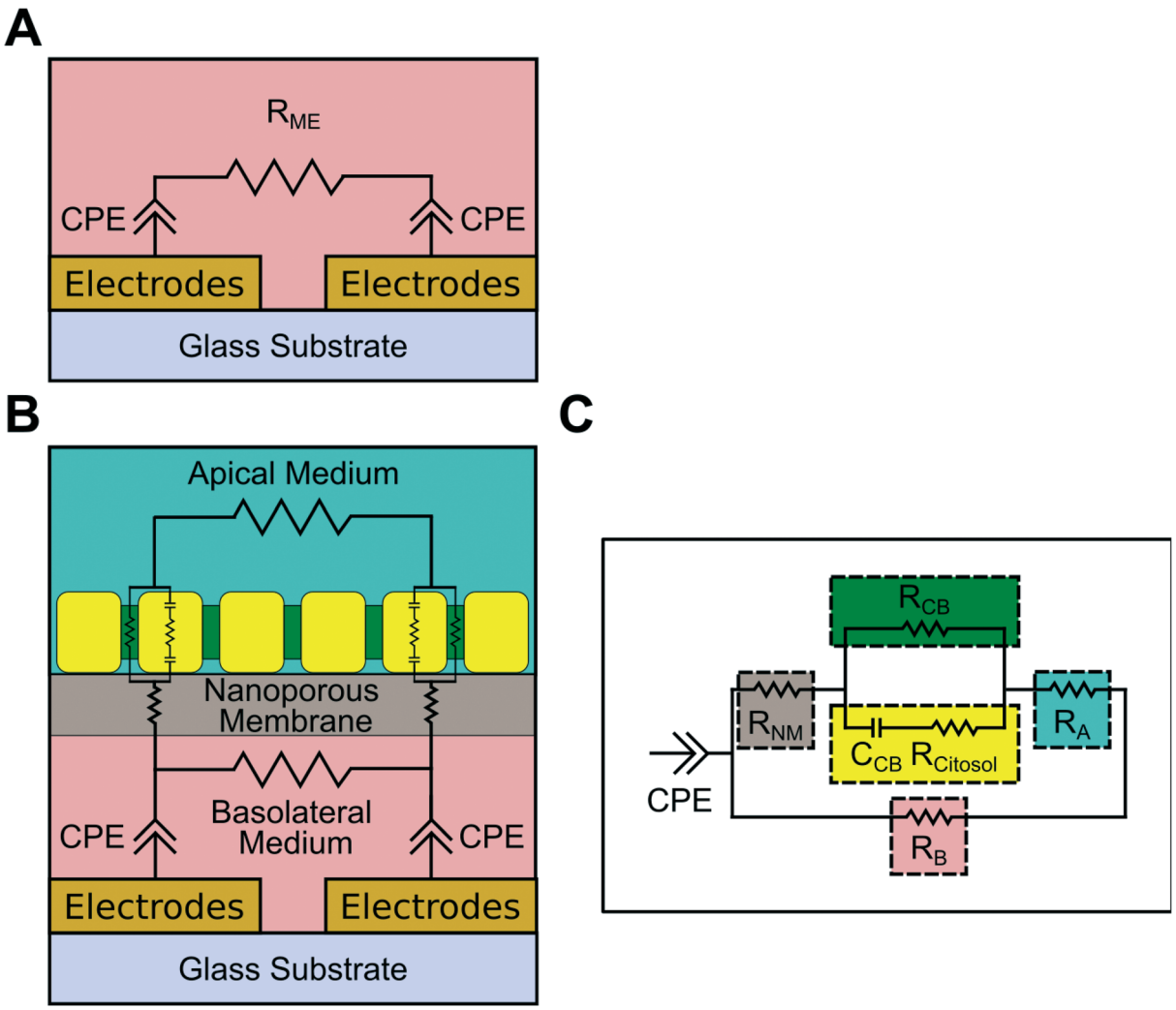

Fig. 3 Equivalent electrical circuit for (A) the media electrodes and (B) the cell electrodes. R_{ME} in (A) represents the medium resistance measured and CPE the constant phase element for the electrode double layer capacitance. A simplified circuit model for the cell electrodes circuit is shown in (C), with R_{NM} the nanoporous membrane resistance, R_{CB} the cell layer paracellular resistance, C_{CB} the epithelial cell layer capacitance and R_A and R_B the medium resistance for the apical and basolateral compartments, respectively.

(Fig. 3A) reduce the uncertainty in the analysis by providing an independent measurement of the electrical properties of the media (conductivity and permittivity), which varies with temperature and salt concentration. At low frequencies (10^3 Hz), the contribution to the circuit from the permittivity of the medium is insignificant and is ignored, hence only the medium resistance is shown in the figure. These electrodes also provide the parameters of the electrical double layer of the electrodes, modelled as a constant phase element (CPE), see Fig. 3(B and C). The basal compartment resistance (R_B), and the nanoporous membrane with the epithelial cell layer are modelled as a parallel combination of cell resistance and capacitance. The apical medium is represented by an additional resistor (R_A). In order to maximise the sensitivity of the system to changes in cell electrical properties the value of R_B should be maximum, *i.e.*, minimum current flow through the basolateral layer. This is achieved by making the height of the microfluidic channel as small as possible. In this work it was set to 275 μm which provides a trade-off between sensitivity and a reasonable volumetric flow of liquid beneath the cells with an appropriate flow velocity. From this equivalent circuit the electrical parameters of the cell layer can be determined.

1.1.2 Electrical model. The constant phase element (CPE) accounts for the frequency dependence of the electrical double layer impedance, defined by eqn (1).

$$Z_{CPE} = \frac{1}{Q_M(j\omega)^{\alpha_M}} \quad (1)$$

If the impedance is a pure capacitance the CPE exponent (α_M) is equal to 1, and a pure resistance is equal to 0. For most metal (or metal oxide) electrodes the exponent varies between 0.5 and 0.9. The magnitude of the impedance is defined by the parameter Q_M. For the low frequency (10^3 to 10^5 Hz) range used in these experiments the media

impedance approximates to the resistance, and so the measured impedance of the 'media electrodes' is simply the sum of the CPE and medium resistance, seen in eqn (2). Although there are two Z_{CPE} in the model, one for each electrode, for simplicity these are represented as a single value in the equation.

$$Z_{\text{Media Electrode}} = Z_{CPE} + R_M \quad (2)$$

The cell chamber consists of two compartments separated by the high porosity membrane. Each compartment, basolateral and apical, has a medium resistance of R_B and R_A respectively. The cell chamber electrodes provide the resistance of the nanoporous support membrane and cell layer, together with the epithelial cell layer capacitance. All other parameters in this equivalent circuit can be fixed and determined by the media electrodes. The resistance of the nano porous support (R_{SM}) was modelled following Hall *et al.*,[41] where the pores were modelled as cylindrical channels with a fixed conductivity defined by their geometry together with an access resistance. This gives a total pore resistance for the membranes of approximately 13.3 Ω, much smaller than the resistance of other components in the electrical circuit model. Given this is in series with the apical resistance (R_A) the two were assigned a single variable. The cell barrier impedance (Z_{CB}) was modelled as the parallel combination of a resistor (R_{CB}) and a capacitor (C_{CB}) which account for the ohmic resistance of the tight junctions and the capacitive behaviour of the cell membrane respectively.[36] Thus, the cell electrode circuit model is defined by eqn (3). A more detailed list of equations is provided in ESI† detailed equation list.

$$Z_{\text{Cell Electrode}} = Z_{CPE} + \left[\left(2 \times \frac{R_{CB}}{j\omega C_{CB} R_{CB} + 1} + R_A\right)^{-1} + \frac{1}{R_B}\right]^{-1} \quad (3)$$

The electrical parameters were determined from the equivalent circuit using the following algorithm:

1. CPE (Q_M and α_M) and medium resistance (R_{SM}) determined from the 'media electrodes' by fitting to eqn (2).

2. Impedance data from the "cell electrodes" was fitted to eqn (3) using the 3 parameters determined from step 1. To optimise the fit, these parameters were assigned upper and lower boundaries of ±5%.

3. Values for the cell layer resistance and capacitance were determined by curve fitting.

4. Cell layer resistance was multiplied by the nanoporous support membrane surface area to give a TER equivalent (Ω cm^2).

The impedance data are related to the physical properties of the system (conductivity and permittivity) through the electrode chamber geometry. These geometric constants were determined through numerical simulation to be 1.9×10^{-3} m^{-1}, 4.1×10^{-2} m^{-1} and 1.5×10^{-3} m^{-1} for the media electrode, cell electrodes apical and cell electrodes basolateral compartment respectively. For the media electrode, cell electrodes apical and cell electrodes basolateral compartment respectively. For the fit, the CPE exponent (which depends on electrode surface roughness) was assumed to be identical for both sets of electrodes. The CPE magnitude was scaled by the difference in electrode area (factor of 2.3). Apical and basolateral cell media resistance for the cell electrode were determined from the fit for the media electrodes, with the appropriate conversions from differences in geometry (see ESI† detailed equation list). An upper and lower boundary of 5% was applied to the value of apical resistance, since this is affected by the volume of liquid held in the apical compartment, which can vary between chips or over the course of the experiment. A full list of variables and applied boundaries is given in ESI† Table S1.

2 Experimental

Electrodes were fabricated using standard photolithography on 1.1 mm thick glass wafer following the method described by Mingels *et al.*[40] Electrodes were made of 20 nm titanium, 200 nm platinum, 20 nm titanium and 120 nm ruthenium oxide. Following metal deposition, chips were annealed at 420 °C overnight. The microfluidic chip consisted of 3 layers of PMMA either solvent bonded or assembled with 50 μm double-sided adhesive tape (3M). The nanoporous support membrane (Inpore Track Etched Membrane) was adhered to the PMMA chamber with tape, then fixed to the channel layer in a similar manner. The PMMA layers were either machined using a laser cutter or a CNC micro milling machine. Inlet and outlet holes in the glass chips were made with powder blasting. The microfluidic chip was secured onto the manifolds using magnets (10 × 5 × 3 mm) and O-rings. Manifolds were micro-milled from Polyetheretherketone (PEEK). Syringes were connected to the bubble traps (Darwin Microfluidics) with PTFE tubing.

Prior to cell culture, the microfluidic platform was decontaminated by flowing a 1 : 50 sodium hypochlorite solution throughout the system and submerging the apical compartment for 20 minutes. Subsequently the system was copiously rinsed with sterile DI water. Syringes primed with culture media were then attached to the assembly and 100 μL of cell culture media added into the apical compartment of each chip. The system was placed inside a humidified incubator at 37 °C and 5% CO_2 with media pumped at a flow rate of 30 μL per hour overnight to ensure fluidic and electrical stability before introducing cells.

2.1 Cell preparation

The human colorectal carcinoma cell line (Caco-2) and human bronchial epithelial cell line (16HBE14o-) were maintained in Dulbecco's modified Eagle medium (DMEM) or minimal essential medium (MEM) respectively supplemented with 1× Glutamax, 10% foetal bovine serum (FBS), and 1% penicillin/streptomycin. The DMEM was additionally supplemented with 1% sodium pyruvate and 1% non-essential amino acid solution. All cell culture flasks were

coated with 30 μg mL^{-1} collagen (Advanced Biomatrix). For experiments cells were incubated with HBSS without Ca^{2+} and Mg^{2+} for 10 minutes at 37 °C, prior to a 5 minute incubation with 1× trypsin/EDTA solution. Following cell detachment, trypsin was neutralised with complete DMEM or MEM (depending on the cell line) and the cell suspension centrifuged at 300 × *g* for 5 minutes at 20 °C. After discarding the cell-free supernatant, the cell pellet was resuspended in complete medium and counted. Cells were seeded onto collagen coated (30 μg mL^{-1}, 30 min, 37 °C) microfluidic chips at a density of 3×10^5 cells per cm^2 in 100 μL of DMEM or 7.5×10^5 cells per cm^2 in 100 μL of MEM for the Caco-2 and 16HBE14o- cells respectively. The microfluidic chip was left undisturbed in the incubator at 37 °C for 20 hours (Caco-2) or 1 hour (16HBE14o-) to allow cells to adhere to the support membrane. After which, media was perfused through each chip at a flow rate of 30 μL per hour. Additionally, cells were seeded onto collagen coated Transwells® inserts, inside a 24 well-plate with 200 and 500 μL of complete MEM or DMEM in the apical and basolateral compartments respectively. Medium was changed every 2 days and TEER measurements were recorded daily using an EVOM Epithelial Voltohmmeter.

2.2 Reagent preparation

Two different challenge experiments were performed. The first experiment involved apically treating cells with Triton X-100 (TX-100, final 1% solution v/v). The second experiment involved apical stimulation with a synthetic analogue of dsRNA (to mimic viral infection) polyinosinic:polycytidylic acid (Poly I:C, final concentration 25 μg mL^{-1}) (Invivogen) or a corticosteroid, fluticasone propionate (final concentration 100 nM) alone or together in complete MEM media. Complete MEM media was administered apically as a control.

2.3 Immunofluorescent staining

Membranes containing cells were washed with 1× PBS and fixed in 4% PFA for approximately 20 minutes at room temperature, then washed and stored in PBS. Membranes were removed from the chips, transferred to a glass slide, and submerged in blocking buffer (2% BSA, 0.1% Tween-20 in PBS). Permeabilization buffer (0.1% TX-100 in PBS) was then applied to the samples for 15 minutes at room temperature followed by blocking buffer for 1 hour at room temperature. Samples were stained with Acti-stain555-phalloidin (70 nM, Cytoskeleton, PHDH1-A) and AlexaFluor®488-conjugated mouse anti-human occludin antibody (2.5 μg mL^{-1}, Life Technologies, Clone OC-3F10) in blocking buffer overnight at 4 °C in a humidified chamber. Samples were then washed in wash buffer (0.1% Tween-20 in PBS) three times, followed by an incubation with the nuclear stain 4′,6-diamidino-2-phenylindole (DAPI, 2 μg mL^{-1} in dH_2O, ThermoFisher) for 15 minutes in the dark. Samples were rinsed with wash buffer followed by dH_2O prior to cover slips being mounted onto slides with Mowiol (Sigma). Samples were aligned (Leica DMI 6000 inverted fluorescence microscope) and images were captured at 63× in *xyz* mode using confocal microscopy (Leica TCS-SP8 laser scanning microscope with the LAS X software (Leica)) using laser wavelengths of 405 nm (DAPI), 561 nm (Actin) and 488 nm (Occludin).

3 Results and discussion

To assess variability between microfluidic chips, MEM cell culture medium was first perfused through all 8 basolateral channels for 12 hours, with 100 μL of media in the apical chamber. Impedance data were collected continuously, with the mean value of the medium resistance and electrode CPE determined from the circuit model. This is summarised in Table 1, which shows that the culture medium resistance and CPE exponent have low standard deviations, with the values of cell medium resistance close to the expected values derived from the numerically calculated geometric cell constants (see below). However, the magnitude of the CPE was more variable, which may be due to variations in the electrode area arising from the manual assembly of the chip and variability in the metal oxide of the electrodes. The culture medium conductivity was measured with a conductivity meter (YSI 3200) as 1.46 S m^{-1}. Based on the calculated geometrical cell constants of the chip and electrodes (see ESI† Geometrical cell constants), using this value of conductivity the cell media resistance should be approximately 390 Ω and 467 Ω for the media and cell electrode chambers respectively.

These values are similar to the experimental values (Table 1). Impedance measurements were made for chips with and without a nanoporous support membrane. At 1 kHz, the resistance differed by approximately 28 Ω, a value close to the calculated value for the resistance of the membrane, and negligible compared to the medium resistance.

3.1 Cell culture

The Caco-2 colorectal epithelial cell line[19,42–46] was grown on individual chips for 5 days with media flowing beneath the support membrane, and EIS data acquired every 17 minutes. Examples of daily impedance spectra (phase angle and magnitude) are shown in Fig. 4. The circuit model was first used to determine the electrode CPE and medium resistance, then using eqn (3) the epithelial barrier resistance and capacitance. Values for the medium resistance and electrode CPE are given in the ESI.† *R*-Squared values were calculated for the modelled data; see ESI† Fig. S4 and S5. Examples of equivalent TER and cell layer capacitance (determined from each impedance spectrum) are shown in Fig. 5.

The cell layer resistance and capacitance increased over the course of 5 days, reaching an average of 207 ± 59 Ω cm^2 and 1.97 ± 0.13 μF cm^{-2} respectively. The perturbation seen at day 1 for Caco-2 cells coincides with initiation of basolateral perfusion, since these cells required 24 hours to fully adhere unlike the 16HBE14o- cells which only required

Table 1 Values of electrical parameters for the cell culture medium determined from impedance measurements over a duration of 12 hours. The average and standard deviation for culture medium resistance (or apical resistance for the cell electrodes), CPE magnitude and CPE exponent is shown for a set of 8 microfluidic chips over 12 hours

	Culture medium resistance (Ω)	Media electrode			Cell electrode	
		CPE magnitude	CPE exponent	Apical resistance (Ω)	CPE magnitude	CPE exponent
Average	376	4.2×10^{-5}	0.6	467	9.2×10^{-5}	0.64
Standard deviation	14.0 (3.7%)	1.19×10^{-5} (28.3%)	0.04 (6.7%)	18.8 (4.0%)	3.1×10^{-5} (34%)	0.04 (6.3%)

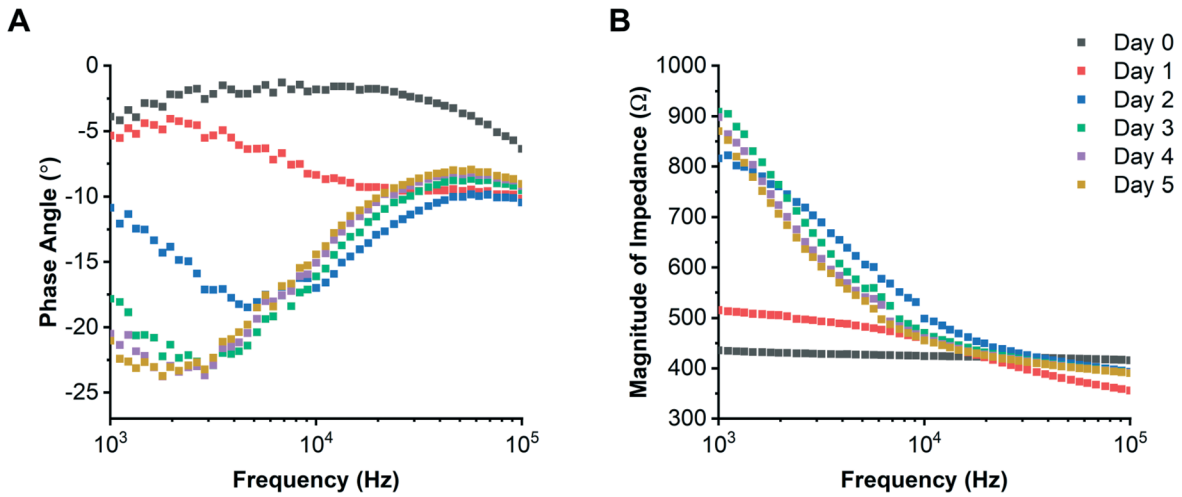

Fig. 4 Example experimental impedance spectra showing changes in phase (A) and magnitude (B) with time as the Caco-2 cells polarise creating an electrically insulating barrier. Each coloured line representing a different day. Data are from a single microfluidic chip and are representative of 8 chips in parallel.

1 hour. Epithelial cell barrier capacitance increased over time and was similar to values reported by Helm *et al.*,[34] (approximately 2 μF cm^{-2} after 5 days of culture with flow). This increase has previously been attributed to formation of microvilli.[34] For comparison, Caco-2 cells were also grown in standard Transwell® inserts where they developed a TER of 1258 ± 40 Ω cm^2 over 5 days of culture. The difference in TER observed between the microfluidic system and static Transwell® cultures has been reported previously,[34] where cells cultured in a fluidic system have a lower TER: 200 Ω cm^2 compared with 600 Ω cm^2 for no flow. Azizgolshani *et al.*,[47] also showed that the TER of Caco-2 cells grown with flow was approximately 200 Ω cm^2 after 11 days of culture. Our data shows a lower TER with flow, consistent with previous publications.

To compare the response of epithelial cells from a different tissue, bronchial epithelial cells (16HBE14o-) were cultured for 5 days with flow. Example daily impedance spectra (phase angle and impedance magnitude) are shown in Fig. 6; values of electrode CPE and medium resistance are given in the ESI† along with *R*-squared values (see ESI† Fig. S6 and S7) For this cell type, cell layer resistance and capacitance reached an average of 418 ± 121 Ω cm^2 and 0.13 ± 0.02 μF cm^{-2} after 5 days of culture. The epithelial cell layer capacitance (Fig. 7A) stabilised quickly to approximately 0.13 ± 0.02 μF cm^{-2} (day 0.5) after initial cell seeding (day 0), probably because the cells were seeded at a high density (unlike the Caco-2 cells which were seeded at a lower density). The 16HBE14o- cell layer capacitance is smaller than reported for other cell layers which are typically in the range of 1–4 μF cm^{-2}.[32,36,48] Caco-2 cells have been shown to develop microvilli, which would lead to a higher capacitance[27,34] but the 16HBE14o- cells stack on top of one another (see ESI† Fig. S8), which would result in a lower value of cell layer capacitance.

The cell layer resistance increased throughout the experiment, reaching an average peak value of 418 ± 121 Ω cm^2 on day 5 (Fig. 7B). This barrier resistance was almost double the value obtained with the Caco-2 cells, highlighting the ability of the device to demonstrate cell type-related differences in barrier permeability. The same bronchial epithelial cells were also grown (in parallel) on commercial Transwell® inserts. This gave a day 5 average TER of 803 ± 34 Ω cm^2, consistent with reported values for cells grown without flow (between 330–2500 Ω cm^2 (ref. 10, 15 and 49)). These data indicate that the TER in the microfluidic device with flow are lower than no-flow, similar to the findings with the Caco-2 cell line. This is supported by previous studies with polarized 16HBE14o- cells where a lower TER was measured in cells on Transwell® inserts with flow (560 Ω cm^2)[50] and in cells perfused in Ussing chambers (TER of 105 Ω cm^2).[51] It is likely that these differences under flow have a biological explanation. For example, tight junctions can participate in the regulation of

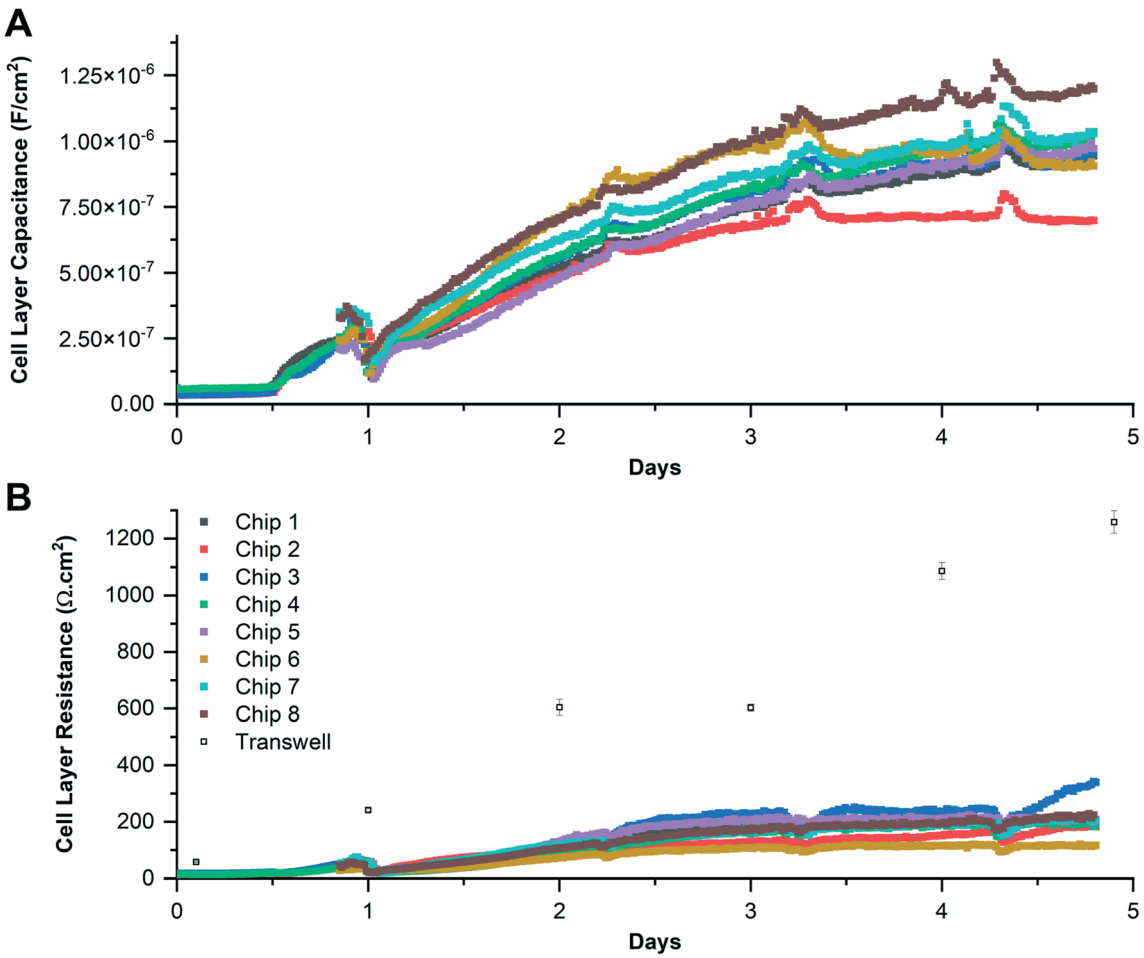

Fig. 5 Epithelial cell layer capacitance (A) and resistance (B) for Caco-2 cells grown in the microfluidic chip. Epithelial cell layer capacitance and resistance (B) were calculated assuming a support membrane surface area of 0.2 cm^2. Data are from 8 individual microfluidic chips run in parallel and the average TER of 2 individual Transwell® static cultures, with error bars representing the standard deviation.

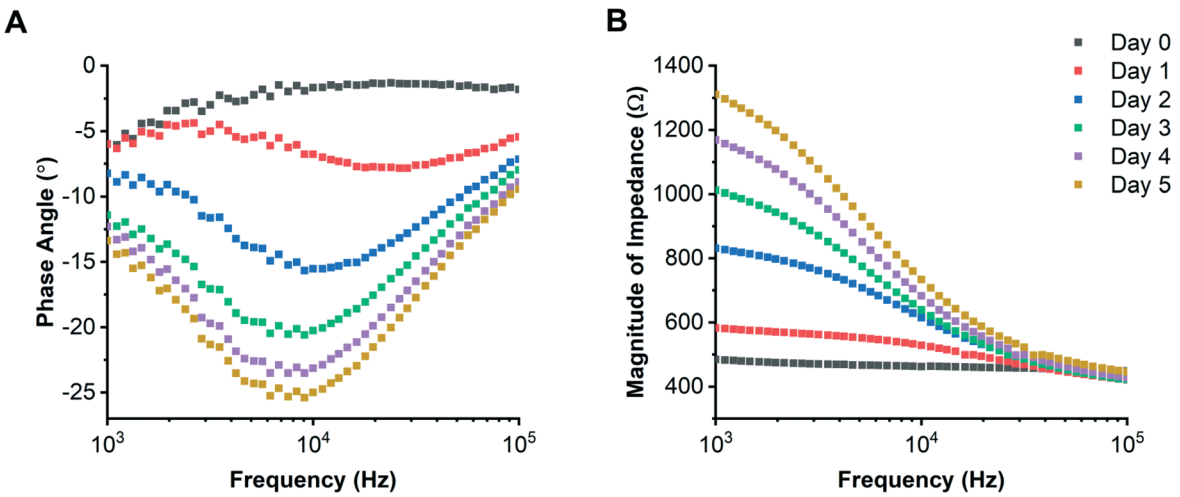

Fig. 6 Example impedance spectra for 16HBE14o- cells showing changes in phase (A) and magnitude (B) as a function of time consistent with the formation of tight junctions and an electrically insulating barrier. Each coloured line representing a different day. Data is from a single microfluidic chip and are representative of 8 chips in parallel.

the mechanical properties of epithelial monolayers and are finely tuned by the contractility of the actomyosin cytoskeleton,[52] a highly dynamic structure that is sensitive to shear stress.[53] Actomyosin contractility is required both

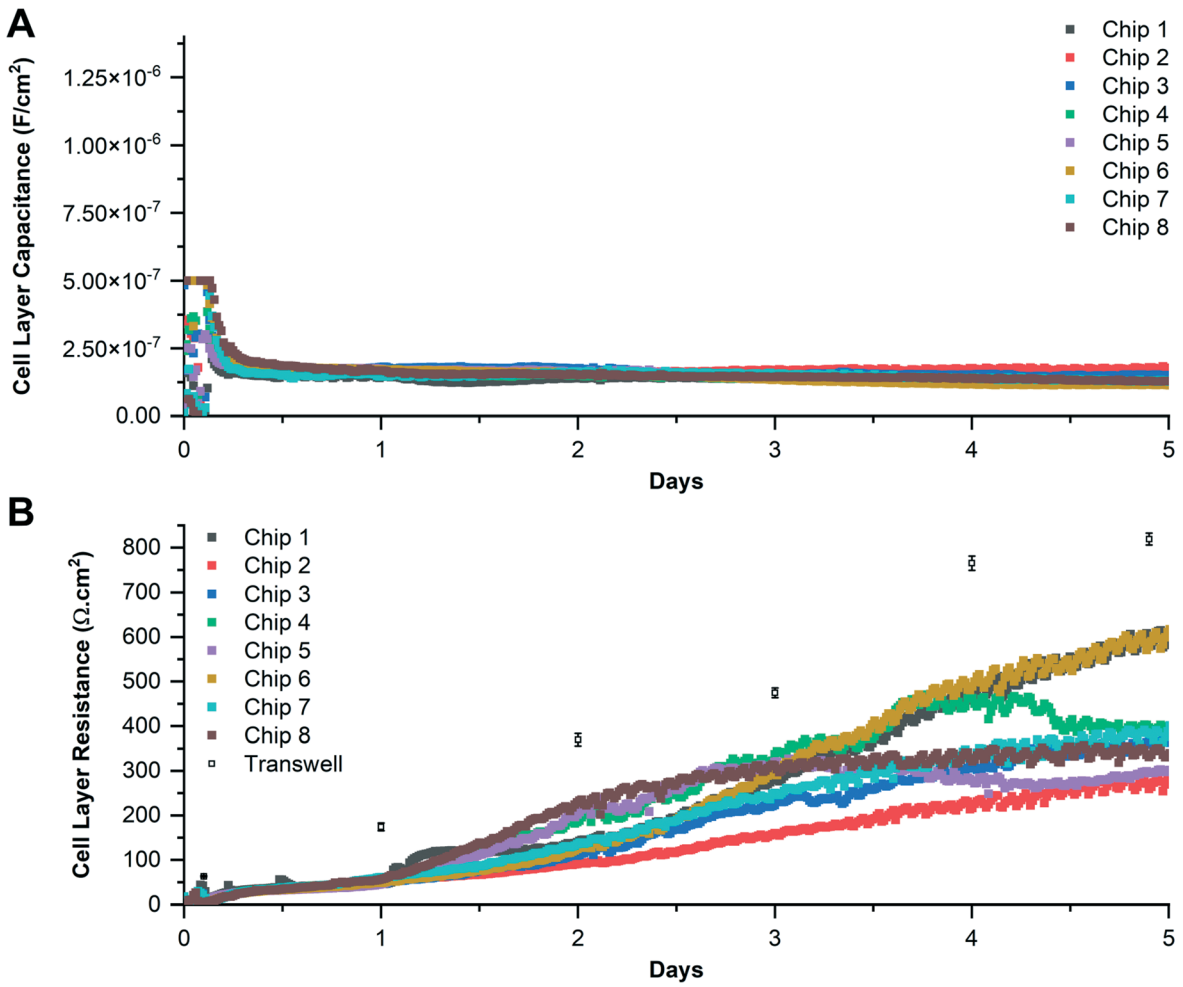

Fig. 7 Epithelial cell layer capacitance and resistance extracted by curve fitting the impedance data for 16HBE14o- cells grown over time on microfluidic chips. Epithelial cell layer capacitance (A) and resistance (B) were calculated assuming a cell culture membrane surface area of 0.2 cm^2. Data are from 8 individual microfluidic chips run in parallel and the average TER of 4 individual Transwell® static cultures. Transwell data is the average of 4 separate wells, with error bars representing the standard deviation.

to allow claudins fibrils to operate correctly, and to reinforce the actin cytoskeleton to prevent leaks.[52]

3.2 Apical challenge

The 16HBE14o- cells were grown for 5 days with a flow rate of 30 μL per hour. After formation of the epithelial barrier, cells were then apically exposed to 1% TX-100.[36] This caused an immediate disruption of the epithelial barrier, evidenced by the sharp drop in the normalised TER from 100% to 0%, as compared with control chips without TX-100 (Fig. 8A). To extend the barrier challenge into a more physiologically relevant context, viral infection was simulated by challenging cells with a dsRNA viral analogue Poly I:C (25 μg mL^{-1}). dsRNA is produced during replication of RNA viruses and is a pathogen-associated molecular pattern detectable by pattern recognition receptors within infected cells. It triggers an anti-viral response including inflammation, disassembly of tight junctional complexes and actin cytoskeleton reorganization without cell apoptosis. Reorganization leads to an increase in barrier permeability, leading to a decrease in TER.[8] Within the microfluidic chip, addition of medium to the apical compartment caused an initial perturbation in the cell barrier irrespective of whether the medium contained dsRNA, or corticosteroid (Fig. 8B). This may be due to small mechanical perturbations and/or temperature fluctuations during introduction of the challenge even though the cells remain in the incubator. This effect was not visible for the TX-100 experiment, as the incubator was open for less time during stimulation, minimizing the temperature drop. When the challenge medium also contained dsRNA, the TER dropped quickly, reaching a minimum 8 hours after challenge. Addition of a corticosteroid (fluticasone propionate) in combination with dsRNA reduced the severity of the drop in TER in the initial hours after introducing the stimulus, which then stabilised to approximately 25% of the initial value. This is consistent with Transwell® data (Fig. 8C), where the addition of the corticosteroid mitigates the barrier disrupting effect of dsRNA.[54]

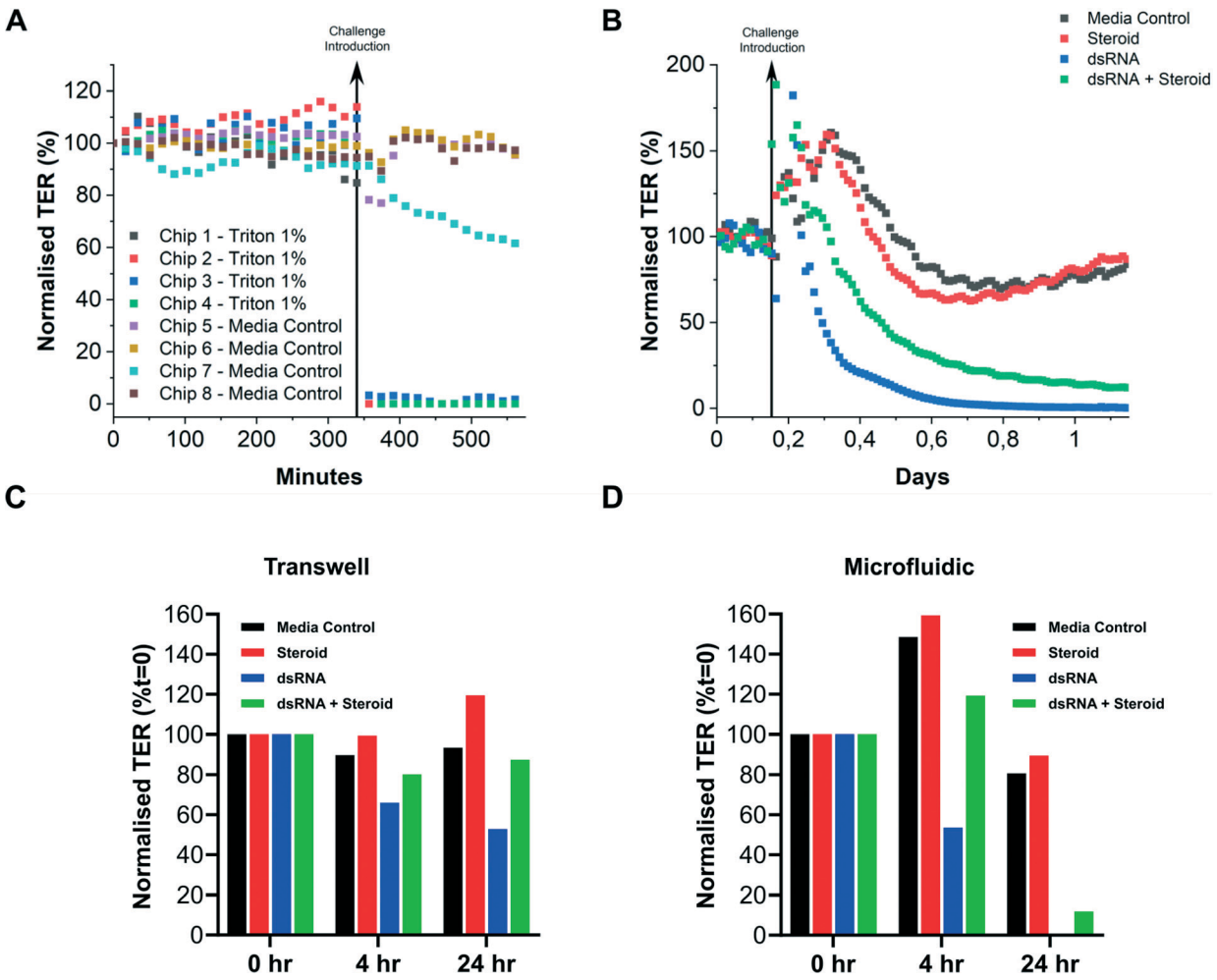

Fig. 8 Effect of TX-100, corticosteroid or dsRNA challenge on 16HBE14o- cells grown on microfluidic chips. Plots of TER for two separate apical stimuli experiments extracted from the impedance spectrum for the microfluidic chip. (A) Normalised TER data from the platform for TX-100 apical stimulation; each coloured line represents a different chip. (B) Normalised TER data for steroid (red), dsRNA (blue) and dsRNA + steroid (green) apical stimulations, with media control (black). Each data point determined by circuit modelling from the impedance spectrum at each measurement point and each line represents the average of duplicate conditions. The vertical black line is the time point of apical stimulation. (C) and (D) Show TER data from a static Transwell and microfluidic cultures respectively for steroid (red), dsRNA (blue) and dsRNA + steroid (green) apical stimulations, with media control (black). Data for TX-100 are for one biological repeat, with 4 chips per condition. Data for corticosteroid and dsRNA stimulation are one biological repeat, with 2 chips or Transwell inserts per condition.

Immunofluorescence staining supported the EIS findings. Compared to control cells (Fig. 9A) which showed pericellular staining for occludin at cell junctions and a well organised actin cytoskeleton, cells treated with dsRNA (Fig. 9B) exhibited occludin reorganisation to the cell–cell junctions, although the cell layer was still intact, as evidenced by the presence of regular DAPI stained nuclei and an actin cytoskeleton. Treatment of cells with dsRNA in the presence of a corticosteroid (Fig. 9D) decreased the impact of dsRNA on the integrity of the epithelial cell barrier, with an improvement in the junctional staining for occludin compared with dsRNA alone. These findings are similar to those of Heijink *et al.*,[54] where fluticasone (500 μg) was able to limit barrier disruption following dsRNA (12.5 μg mL^{-1}) addition to 16HBE14o- cells grown on Transwell supports.

4 Conclusions

We have described a novel multi-channel microfluidic platform with integrated impedance measuring capability for real-time analysis of barrier function by TER. The platform combines plug and play fluidic and electrical functionality suitable for multidisciplinary use (discovery research, target discovery, drug testing, toxicological testing *etc.*) generating a more physiological relevant environment compared to conventional static cultures.

Conventional TER measurements are usually obtained using chop-stick electrodes in a transformation which requires a submerged apical compartment which is unsuitable for ALI cultures. Furthermore, periodic removal from the incubator disrupts the physiological environment and is problematic for temperature sensitive cells.[10]

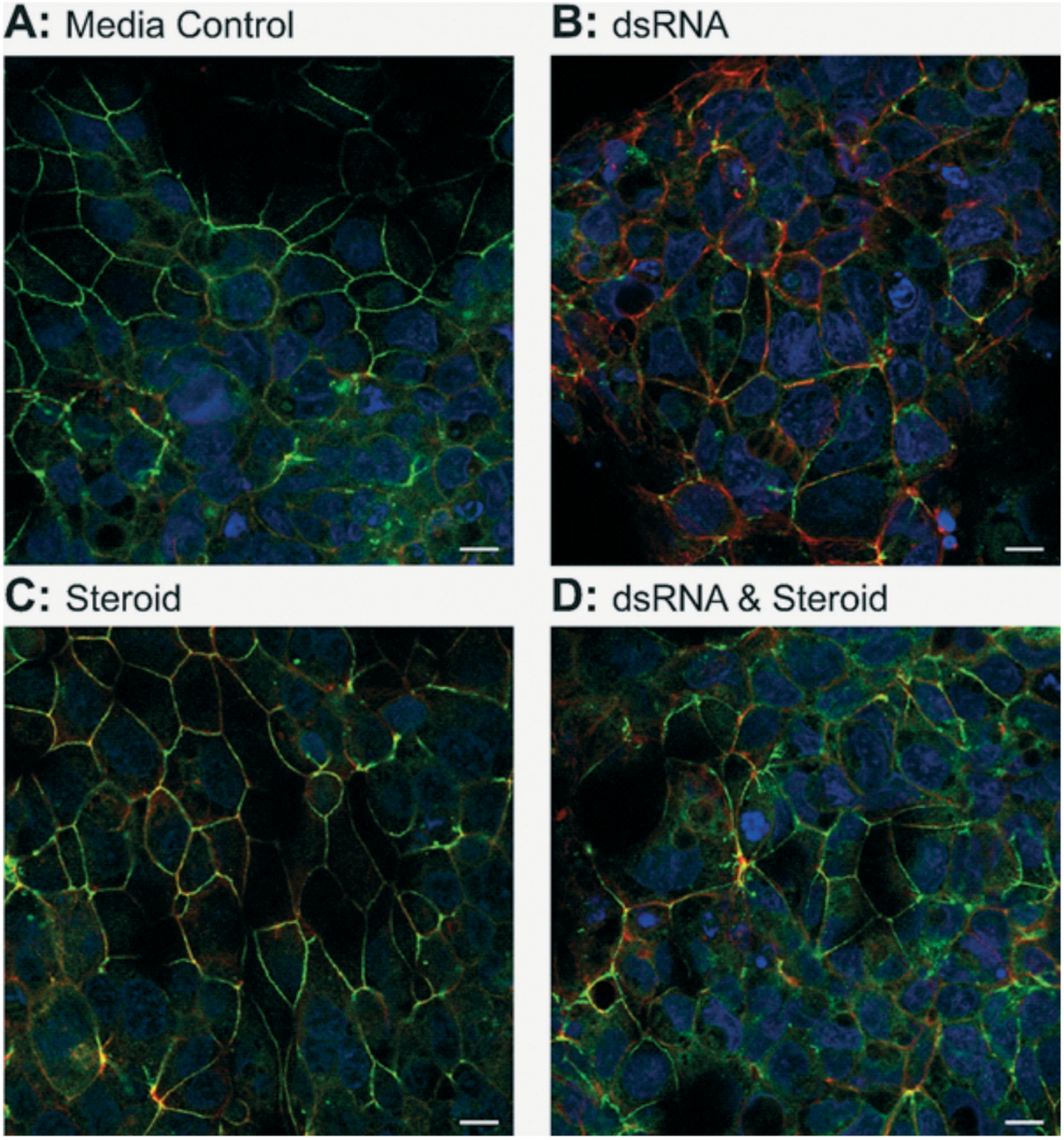

Fig. 9 Visualisation of tight junction distribution 16HBE14oe- cells grown and challenged with dsRNA and corticosteroid on microfluidic chips. Images of one plane from a Z-projection stack with DAPI nuclear (blue), actin cytoskeleton (red) and occludin tight junction staining (green) for 16HBE14o- cells challenged with either media only (A), 25 μg mL^{-1} dsRNA (B), 100 nM corticosteroid (C) or a combination of both dsRNA and corticosteroid (D). Z projection stack captured using confocal imaging at 63× at wavelengths 405 nm (DAPI), 561 nm (actin) and 488 nm (Occludin) (Leica TCS laser scanning microscope). White scale line indicates 10 μm. Data are one biological repeat in duplicate.

Impedance spectroscopy with fixed cis orientation electrodes minimises user-error and significantly reduces these issues. The system has individual perfusion to deliver media to and remove waste from cells at a physiological flow rate synonymous with interstitial flow. This is particularly beneficial for down-stream analysis of mediators, providing the opportunity for collection of samples with a temporal resolution if required in the future.

The system uses 2 pairs of electrodes to measure the medium and cell layer impedance separately. A simple circuit model extracts the cell barrier electrical properties from the impedance data to give an equivalent TER enabling comparison with conventional static cultures. Real-time impedance measurements and calculated TER were utilised to analyse the growth and polarisation of Caco-2 and 16HBE14o- cells over 5 days with a continuous microfluidic

flow (30 μL per hour), demonstrating an increase in TER over time. Cells challenged with compounds after 5 days of growth were monitored continuously over time. Dissolution of the cell membrane by addition of Triton-X-100 led to the immediate disruption of barrier integrity while the addition of dsRNA (Poly I:C 25 μg mL^{-1}) caused a time-dependent decrease in barrier integrity as a result of tight junction disassembly, where the response was modulated by a corticosteroid (fluticasone (100 nM)), consistent with previous findings.[54–56]

The development of a barrier on a chip platform with a tuneable microfluidic flow providing individual perfusion along with the ability to measure barrier integrity in real-time through integrated impedance electrodes provides a distinct advantage over other platforms. This platform is scalable and easy to use with a simple chip to manifold interface. It has the potential to be used in drug development and testing, where the influence of compounds can be analysed in a temporal fashion, facilitating the delivery of new treatments for disease. The platform can analyse eight separate cultures in parallel and can be scaled with 32 chips in a single incubator, enabling testing of several different compounds simultaneously. Future work requires optimisation in the fabrication methodology to decrease chip-to-chip variability, and studies of both submerged and ALI cell barriers with human primary cells.

Data accessibility

All data supporting this study is openly available from the University of Southampton repository at **https://doi.org/10.5258/SOTON/D2138**.

Author contributions

Author contributions are as follows: João Fernandes was involved in the conceptualization, data curation, formal analysis, investigation, methodology, resources, software, validation and writing – original draft; Nikita Karra was involved in the conceptualization, data curation, formal analysis, investigation, methodology, resources, validation and writing – original draft; Joel Bowring was involved in resources and software, Riccardo Reale was involved in conceptualization; Jonathan James was involved in resources and methodology; Cornelia Blume was involved in supervision and resources; Theresa J. Pell was involved in funding acquisition and project administration; Wendy C. Rowan was involved in funding acquisition and project administration; Donna E. Davies was involved in supervision, resources and writing – review and editing; Emily J. Swindle was involved in conceptualization, supervision, funding acquisition, project administration, resources and writing – review and editing; Hywel Morgan was involved in conceptualization, supervision, funding acquisition, project administration, resources and writing – review and editing.

Conflicts of interest

There are no conflicts to declare.

Acknowledgements

This work was funded by the EPSRC, GlaxoSmithKline, IUK (102522) and the Asthma Allergy and Inflammation Research charity. We would like to thank Katie Chamberlain for her assistance with fabrication of glass chips, Mark Long, Anthony Gardener and Jamie Stone for their technical assistance with micro milling and 3D printing and David Johnstone for his support with confocal microscopy. 16HBBE14o- cells were gifted from Prof. D.C. Gruenert, San Francisco, USA. Caco-2 cells were gifted by Prof. P. Calder and provided by his PhD student Luke Dirkin, University of Southampton, UK.

Notes and references

1 A. M. Marchiando, W. V. Graham and J. R. Turner, *Annu. Rev. Pathol.: Mech. Dis.*, 2010, **5**, 119–144.
2 S. Tsukita, M. Furuse and M. Itoh, *Nat. Rev. Mol. Cell Biol.*, 2001, **2**, 285–293.
3 G. Krause, L. Winkler, S. L. Mueller, R. F. Haseloff, J. Piontek and I. E. Blasig, *Biochim. Biophys. Acta, Biomembr.*, 2008, **1778**, 631–645.
4 M. K. Findley and M. Koval, *IUBMB Life*, 2009, **61**, 431–437.
5 E. E. Schneeberger and R. D. Lynch, *Am. J. Physiol.*, 2004, **286**, C1213–C1228.
6 C. Xiao, S. M. Puddicombe, S. Field, J. Haywood, V. Broughton-Head, I. Puxeddu, H. M. Haitchi, E. Vernon-Wilson, D. Sammut, N. Bedke, C. Cremin, J. Sones, R. Djukanović, P. H. Howarth, J. E. Collins, S. T. Holgate, P. Monk and D. E. Davies, *J. Allergy Clin. Immunol.*, 2011, **128**, 549–556.e12.
7 K. Sweerus, M. Lachowicz-Scroggins, E. Gordon, M. LaFemina, X. Huang, M. Parikh, C. Kanegai, J. V. Fahy and J. A. Frank, *J. Allergy Clin. Immunol.*, 2017, **139**, 72–81.e1.
8 F. Rezaee, N. Meednu, J. A. Emo, B. Saatian, T. J. Chapman, N. G. Naydenov, A. De Benedetto, L. A. Beck, A. I. Ivanov and S. N. Georas, *J. Allergy Clin. Immunol.*, 2011, **128**, 1216.
9 Y. Soini, *Respir. Res.*, 2011, **12**, 70–70.
10 P. J. Callaghan, B. Ferrick, E. Rybakovsky, S. Thomas and J. M. Mullin, *Biosci. Rep.*, 2020, **40**, 1–16.
11 L. S. Poritz, L. R. Harris, A. A. Kelly and W. A. Koltun, *Dig. Dis. Sci.*, 2011, **56**, 2802–2809.
12 F. M. Carlier, C. de Fays and C. Pilette, *Front. Physiol.*, 2021, **12**, 1–27.
13 D. W. Powell, *Am. J. Physiol.*, 1981, **4**, 275–288.
14 B. Srinivasan, A. R. Kolli, M. B. Esch, H. E. Abaci, M. L. Shuler and J. J. Hickman, *J. Lab. Autom.*, 2015, **20**, 107–126.
15 C. Blume, R. Reale, M. Held, T. M. Millar, J. E. Collins, D. E. Davies, H. Morgan and E. J. Swindle, *PLoS One*, 2015, **10**, 1–13.

16 R. S. Tavares, T. Phuong-Tao, I. Maschmeyer, S. S. Maria-Engler, M. Schäfer-Korting, A. Winter, C. Zoschke, R. Lauster, U. Marx and L. R. Gaspar, *Int. J. Pharm.*, 2020, **589**, 119788.
17 G. Sriram, M. Alberti, Y. Dancik, B. Wu, R. Wu, Z. Feng, S. Ramasamy, P. L. Bigliardi, M. Bigliardi-Qi and Z. Wang, *Mater. Today*, 2018, **21**, 326–340.
18 M. Wufuer, G. H. Lee, W. Hur, B. Jeon, B. J. Kim, T. H. Choi and S. H. Lee, *Sci. Rep.*, 2016, **6**, 1–12.
19 N. Ashammakhi, R. Nasiri, N. R. de Barros, P. Tebon, J. Thakor, M. Goudie, A. Shamloo, M. G. Martin and A. Khademhosseni, Gut-on-a-chip: Current progress and future opportunities, *Biomaterials*, 2020, **255**, 120196.
20 D. Huh, B. D. Matthews, A. Mammoto, M. Montoya-Zavala, H. Y. Hsin and D. E. Ingber, *Science*, 2010, **328**, 1662–1668.
21 A. M. Ghaemmaghami, M. J. Hancock, H. Harrington, H. Kaji and A. Khademhosseini, *Drug Discovery Today*, 2012, **17**, 173–181.
22 T. Nguyen, S. H. Jung, M. S. Lee, T. E. Park, S. K. Ahn and J. H. Kang, *Lab Chip*, 2019, **19**, 3706–3713.
23 J. W. Song, J. Paek, K. T. Park, J. Seo and D. Huh, *Biomicrofluidics*, 2018, **12**, 042211.
24 M. Humayun, C.-W. Chow and E. W. K. Young, *Lab Chip*, 2018, **18**, 1298–1309.
25 A. Doryab, G. Amoabediny and A. Salehi-Najafabadi, *Biotechnol. Adv.*, 2016, **34**, 588–596.
26 N. Karra, E. Swindle and H. Morgan, *Organs-on-a-Chip*, 2019, **1**, 100002.
27 T. Gerasimenko, S. Nikulin, G. Zakharova, A. Poloznikov, V. Petrov, A. Baranova and A. Tonevitsky, *Front. Bioeng. Biotechnol.*, 2020, **7**, 474.
28 E. Ferrari, C. Palma, S. Vesentini, P. Occhetta and M. Rasponi, *Biosensors*, 2020, **10**, 110.
29 T. Sun and H. Morgan, *Microfluid. Nanofluid.*, 2010, **8**, 423–443.
30 T. Sun, S. Tsuda, K. P. Zauner and H. Morgan, *Biosens. Bioelectron.*, 2010, **25**, 1109–1115.
31 Y. B. Arlk, M. W. Van Der Helm, M. Odijk, L. I. Segerink, R. Passier, A. Van Den Berg and A. D. Van Der Meer, *Biomicrofluidics*, 2018, **12**, 042218.
32 M. Odijk, A. D. Van Der Meer, D. Levner, H. J. Kim, M. W. Van Der Helm, L. I. Segerink, J. P. Frimat, G. A. Hamilton, D. E. Ingber and A. Van Den Berg, *Lab Chip*, 2015, **15**, 745–752.
33 N. Zhang, F. Stauffer, B. R. Simona, F. Zhang, Z. M. Zhang, N. P. Huang and J. Vörös, *Biosens. Bioelectron.*, 2018, **112**, 149–155.
34 M. W. van der Helm, O. Y. F. Henry, A. Bein, T. Hamkins-Indik, M. J. Cronce, W. D. Leineweber, M. Odijk, A. D. van der Meer, L. I. Segerink, D. E. Ingber, J. C. T. Eijkel, M. J. Cronce, M. Odijk, A. Bein, W. D. Leineweber, A. D. van der Meer, A. van den Berg, M. W. van der Helm, D. E. Ingber, T. Hamkins-Indik, L. I. Segerink and O. Y. F. Henry, *Lab Chip*, 2019, **19**, 452–463.
35 F. A. Alexander, S. Eggert and J. Wiest, *Genes*, 2018, **9**, 114.
36 T. Sun, E. J. Swindle, J. E. Collins, J. A. Holloway, D. E. Davies, H. Morgan, E. Davies, H. Morgan, D. E. Davies and H. Morgan, *Lab Chip*, 2010, **10**, 1611–1617.
37 Y. Mermoud, M. Felder, J. D. Stucki, A. O. Stucki and O. T. Guenat, *Sens. Actuators, B*, 2018, **255**, 3647–3653.
38 P. R. Harvey, R. Tarran, S. Garoff and M. M. Myerburg, *Am. J. Respir. Cell Mol. Biol.*, 2011, **45**, 592–599.
39 R. Reale, *Ph.D. thesis*, University of Southampton, 2017.
40 R. Mingels, S. Kalsi, Y. Cheong and H. Morgan, *Sens. Actuators, B*, 2019, **297**, 126779.
41 J. E. Hall, Access resistance of a small circular pore, *J. Gen. Physiol.*, 1975, **66**, 531–532.
42 K. Verhoeckx, P. Cotter, I. López-Expósito, C. Kleiveland, T. Lea, A. Mackie, T. Requena, D. Swiatecka and H. Wichers, *The impact of food bioactives on health: In vitro and Ex Vivo models*, Springer, 2015, pp. 1–327.
43 L. Wang, J. Wu, J. Chen, W. Dou, Q. Zhao, J. Han, J. Liu, W. Su, A. Li, P. Liu, Z. An, C. Xu and Y. Sun, *Talanta*, 2021, **226**, 122097.
44 G. Preksha, R. Yesheswini and C. V. Srikanth, *Indian J. Pathol. Microbiol.*, 2021, **64**, S52–S57.
45 S. E. Blutt, J. R. Broughman, W. Zou, X. L. Zeng, U. C. Karandikar, J. In, N. C. Zachos, O. Kovbasnjuk, M. Donowitz and M. K. Estes, *Exp. Biol. Med.*, 2017, **242**, 1633–1642.
46 D. Marrero, F. Pujol-Vila, D. Vera, G. Gabriel, X. Illa, A. Elizalde-Torrent, M. Alvarez and R. Villa, *Biosens. Bioelectron.*, 2021, **181**, 113156.
47 H. Azizgolshani, J. R. Coppeta, E. M. Vedula, E. E. Marr, B. P. Cain, R. J. Luu, M. P. Lech, S. H. Kann, T. J. Mulhern, V. Tandon, K. Tan, N. J. Haroutunian, P. Keegan, M. Rogers, A. L. Gard, K. B. Baldwin, J. C. de Souza, B. C. Hoefler, S. S. Bale, L. B. Kratchman, A. Zorn, A. Patterson, E. S. Kim, T. A. Petrie, E. L. Wiellette, C. Williams, B. C. Isenberg and J. L. Charest, *Lab Chip*, 2021, **21**, 1454–1474.
48 G. Linz, S. Djeljadini, L. Steinbeck, G. Köse, F. Kiessling and M. Wessling, *Biosens. Bioelectron.*, 2020, **165**, 112345.
49 D. Papazian, P. A. Würtzen and S. W. K. Hansen, *Int. Arch. Allergy Immunol.*, 2016, **170**, 1–21.
50 C. Blume, R. Reale, M. Held, M. Loxham, T. M. Millar, J. E. Collins, E. J. Swindle, H. Morgan and D. E. Davies, *Immun., Inflammation Dis.*, 2017, **5**, 45–56.
51 A. L. Cozens, M. J. Yezzi, K. Kunzelmann, T. Ohrui, L. Chin, K. Eng, W. E. Finkbeiner, J. H. Widdicombe and D. C. Gruenert, *Am. J. Respir. Cell Mol. Biol.*, 1994, **10**, 38–47.
52 S. Citi, *Biophys. Rev.*, 2019, **11**, 783–793.
53 N. M. Cronin and K. A. DeMali, *Biology*, 2021, **11**, 52.
54 I. H. Heijink, M. R. Jonker, M. de Vries, A. J. van Oosterhout, E. Telenga, N. H. ten Hacken, D. S. Postma and M. van den Berge, *Respir. Res.*, 2016, **17**, 1–13.
55 C. Blume, J. David, R. E. Bell, J. R. Laver, R. C. Read, G. C. Clark, D. E. Davies and E. J. Swindle, *Pathogens*, 2016, **5**, E53.
56 A. Singanayagam, N. Glanville, N. Bartlett and S. Johnston, *Lancet*, 2015, **385**, S88.